THE JOURNAL OF PHYSICAL CHEMISTRY Letters

Letter

Cite This: J. Phys. Chem. Lett. 2018, 9, 3470−3477

pubs.acs.org/JPCL

New Tungsten Borides, Their Stability and Outstanding Mechanical Properties

Alexander G. Kvashnin,*[,†,‡] Hayk A. Zakaryan,[§] Changming Zhao,[∥] Yifeng Duan,[∥] Yulia A. Kvashnina,[†,‡] Congwei Xie,[†,⊥] Huafeng Dong,[#] and Artem R. Oganov*[,†,‡,⊥]

[†]Skolkovo Institute of Science and Technology, Skolkovo Innovation Center, 3 Nobel Street, 143026 Moscow, Russia

[‡]Moscow Institute of Physics and Technology, 9 Institutsky Lane, 141700 Dolgoprudny, Russia

[§]Yerevan State University, 1 Alex Manoogian Street, 0025 Yerevan, Armenia

[∥]School of Physics, China University of Mining and Technology, Xuzhou, Jiangsu 221116, China

[⊥]International Center for Materials Discovery, Northwestern Polytechnical University, Xi'an 710072, China

[#]School of Physics and Optoelectronic Engineering, Guangdong University of Technology, Guangzhou 510006, China

Supporting Information

ABSTRACT: We predict new tungsten borides, some of which are promising hard materials that are expected to be stable in a wide range of conditions, according to the computed composition−temperature phase diagram. New boron-rich compound WB_5 is predicted to be superhard, with a Vickers hardness of 45 GPa, to possess high fracture toughness of ∼4 MPa·m$^{0.5}$, and to be thermodynamically stable in a wide range of temperatures at ambient pressure. Temperature dependences of the mechanical properties of the boron-richest WB_3 and WB_5 phases were studied using quasiharmonic and anharmonic approximations. Our results suggest that WB_5 remains a high-performance material even at very high temperatures.

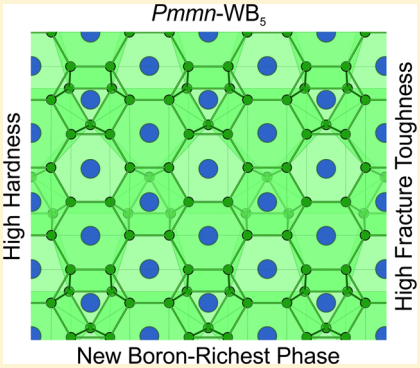

Superhard materials are important for many applications. A material can be called superhard if its Vickers hardness is higher than 40 GPa.[1−3] Well-known hard and superhard materials include carbon allotropes,[4−6] with the hardest possible material being diamond, followed by carbon nitrides, cubic boron nitride, boron allotropes, and borides, nitrides, and carbides of transition metals as such chromium,[7−9] rhenium,[10] molybdenum,[11,12] tungsten,[13−18] etc. Some of these carbides (WC) and nitrides (TiN) are widely used in machining tools and mining, e.g., in drilling equipment.

There are five stable tungsten boride phases known from experiments: W_2B,[13,19] WB (including α and β phases),[19,20] WB_2,[21] and WB_4.[13,14,16] Numerous theoretical investigations of the stability of new possible phases and their physical properties were published recently.[10,15,22,23] Wide ranges of homogeneity of W−B phases were mentioned in theoretical and experimental works,[13,18,24] and at least partly these may be caused by extensive polysomatism (for a discussion of polysomatism, see ref 25). This leads to big difficulties for synthesis of stoichiometric single-crystal phases. Quite often, this leads to inaccurate crystallographic descriptions of synthesized phases by experimental methods, especially given the difficulties in locating positions of light boron atoms using X-ray diffraction. Due to this, the originally claimed W_2B_5 phase[19] was later identified as W_2B_4 with a $P6_3/mmc$ space group.[24,26] For a discussion, we refer to ref 18. Given these difficulties, recently developed crystal structure prediction methods can provide invaluable help.

Here we performed an evolutionary variable-composition search for new stable tungsten borides using the USPEX code.[27−29] All experimentally synthesized phases were found during the search, together with three new stable phases (*Cm*-W_4B_3, *C*2-W_6B_5, *Pm*-W_4B_7, *Pmmn*-WB_5). Thermodynamic stability at different temperatures was examined, Vickers hardness and fracture toughness were evaluated using recently developed models, and temperature-dependent elastic properties were studied for WB_3 and WB_5; these are of special interest, being the boron-richest tungsten borides.

Stable phases in the W−B system were predicted using a first-principles variable-composition evolutionary algorithm (EA) as implemented in the USPEX code.[27−29] For each promising composition, fixed-composition searches were carried out. Here, evolutionary searches were combined with structure relaxations and total energy calculations using density functional theory (DFT)[30,31] within the generalized gradient approximation (Perdew−Burke−Ernzerhof functional)[32] and the projector augmented wave method[33,34] as implemented in

Received: April 20, 2018
Accepted: June 2, 2018
Published: June 2, 2018

Downloaded via Alexander Kvashnin on May 14, 2020 at 13:04:33 (UTC).
See https://pubs.acs.org/sharingguidelines for options on how to legitimately share published articles.

© 2018 American Chemical Society

DOI: 10.1021/acs.jpclett.8b01262
J. Phys. Chem. Lett. 2018, 9, 3470−3477

the VASP[35−37] package. We used the plane-wave energy cutoff of 500 eV, and Γ-centered k-meshes of $2\pi \times 0.05$ Å^{-1} resolution for Brillouin zone sampling, ensuring excellent convergence of total energies. During structure search, the first generation (120 structures) was produced randomly with up to 16 atoms (variable-composition search) and 36 atoms (fixed-composition search) in the primitive unit cell, and succeeding generations were obtained by applying heredity (40%), softmutation (20%), and transmutation (20%) operators, respectively, and 20 and 15% of each generation was produced using symmetric and topological random generators, respectively.

For the predicted crystal structures, we performed high-quality calculations of their physical properties. Crystal structures were relaxed until the maximum net force on atoms became less than 0.01 eV/Å. The Monkhorst−Pack scheme[38] was used to sample the Brillouin zone, using 10 × 10 × 10 ($I4/m$-W_2B), 8 × 8 × 8 (Cm-W_4B_3), 8 × 8 × 8 ($C2$-W_6B_5), 8 × 8 × 8 (Cm-W_8B_7), 10 × 10 × 8 ($P\bar{4}2_1m$-WB), 10 × 10 × 4 ($I4_1/amd$-WB), 6 × 10 × 4 ($Cmcm$-WB), 10 × 6 × 4 (Pm-W_4B_7), 8 × 8 × 4 ($R\bar{3}m$-WB_2), 8 × 8 × 8 ($P\bar{6}m2$-WB_3), 8 × 8 × 8 ($P6_3/mmc$-WB_4), and 8 × 8 × 8 ($Pmmn$-WB_5).

The elastic tensor was calculated using the stress−strain relations:

$$C_{ij} = \frac{\partial \sigma_i}{\partial \eta_j} \tag{1}$$

where σ_i is the ith component of the stress tensor and η_j is the jth component of the strain tensor. Equation 1 can be rewritten in terms of the Helmholtz free energy F as

$$C_{ij} = \frac{1}{V}\frac{\partial^2 F}{\partial \eta_i \partial \eta_j} \tag{2}$$

We compute the Helmholtz free energy as

$$F(T) = E_0(V) + F_{\text{vib}}(V, T) \tag{3}$$

where E_0 is the total energy from the DFT calculations and F_{vib} is vibrational Helmholtz free energy calculated from the following relation in the quasiharmonic approximation[39]

$$F_{\text{vib}}(V, T) = k_B T \int_\Omega g(\omega(V)) \ln\left[1 - \exp\left(-\frac{\hbar\omega(V)}{k_B T}\right)\right] d\omega + \frac{1}{2}\int g(\omega(V))\hbar\omega \, d\omega \tag{4}$$

Here $g(\omega(V))$ is the phonon density of states at the given volume, calculated using the finite displacements method as implemented in PHONOPY,[40,41] with forces computed by VASP.[35−37]

The high melting temperature (>3000 K)[42] of tungsten and tungsten-based materials allows the use of these materials at extremely high temperatures, where the anharmonic part of the free energy is important[39]

$$F(T) = E_0(V) + F_{\text{vib}}(V, T) + F_A(V, T) \tag{5}$$

Here we determined the anharmonic contribution as follows[43]

$$F_A(V, T) \approx A_2 T^2 \tag{6}$$

where, empirically[43]

$$A_2 = \frac{3k_B}{\Theta_H}(0.0078\langle\gamma\rangle - 0.0154) \tag{7}$$

Here Θ_H is the high-temperature harmonic Debye temperature defined as[39]

$$\Theta_H = \frac{\hbar}{k_B}\left(\frac{5}{3}\langle\omega^2\rangle\right)^{1/2} \tag{8}$$

where $\langle\omega^2\rangle$ is the average squared harmonic phonon frequency. In Debye theory, the average Grüneisen parameter $\langle\gamma\rangle$ can be calculated as

$$\langle\gamma\rangle = -\frac{d\ln(\Theta_H)}{d\ln(V)} \tag{9}$$

Using eqs 2 and 5 the temperature-dependent elastic tensor can be calculated as

$$C_{ij}(T) = \frac{1}{V(T)}\frac{\partial^2 F(T)}{\partial \eta_i \partial \eta_j} \tag{10}$$

The Grüneisen parameter can be calculated from the dependence of phonon frequencies on applied pressure using the following relation[44]

$$\langle\gamma\rangle = \langle\gamma_i\rangle = \left\langle \frac{B_0}{\omega_i}\frac{d\omega_i}{dp} \right\rangle \tag{11}$$

where ω_i is the phonon frequency of the ith mode, B_0 is the bulk modulus, p is pressure.

Both eqs 9 and 11 give similar values of the Grüneisen parameter within ±0.08. For example, for pure tungsten, we obtain the average Grüneisen parameters of 1.755 (eq 9) and 1.68 (eq 11), both of which are in good agreement with the experimental value of 1.7 from ref 42. Grüneisen parameters calculated for h-BN (0.09) and c-BN (1.02) are also in agreement with reference data (0.1 and 0.95, respectively).[39]

The Vickers hardness was estimated according to Chen's model[45] (H_V)

$$H_V = 2\cdot(k^2\cdot G)^{0.585} - 3 \tag{12}$$

where k is the Pugh ratio ($k = G/B$), G is the shear modulus, and B is the bulk modulus. The bulk and shear moduli were calculated in GPa via Voigt−Reuss−Hill averaging.[46,47] Test calculations of the Vickers hardness for a number of materials using Chen's model agree well with the reference experimental data: diamond 98 (~96[48]), TiN 22.6 (20.5[49]), c-BN 56.9 (~55[1,50]).

Fracture toughness was calculated using an empirical model from ref 51, where the fracture toughness can be estimated as follows

$$K_{IC} = \alpha\cdot V^{1/6}\cdot G\cdot\left(\frac{B}{G}\right)^{1/2} \tag{13}$$

where α is an enhancement factor accounting for the degree of metallicity, V is the volume per atom in m^3, and G and B are shear and bulk moduli in MPa, respectively.[51] For the case of insulators and semiconductors and also transition metal carbides, nitrides, and borides, $\alpha = 1$.[51] The calculated values of the fracture toughness of diamond, WC, and c-BN are within the range of experimentally measured values and equal to 6.33 MPa·m$^{0.5}$ (4−7 MPa·m$^{0.5}$[52−54]) for diamond, 5.37 MPa·m$^{0.5}$

DOI: 10.1021/acs.jpclett.8b01262
J. Phys. Chem. Lett. 2018, 9, 3470−3477

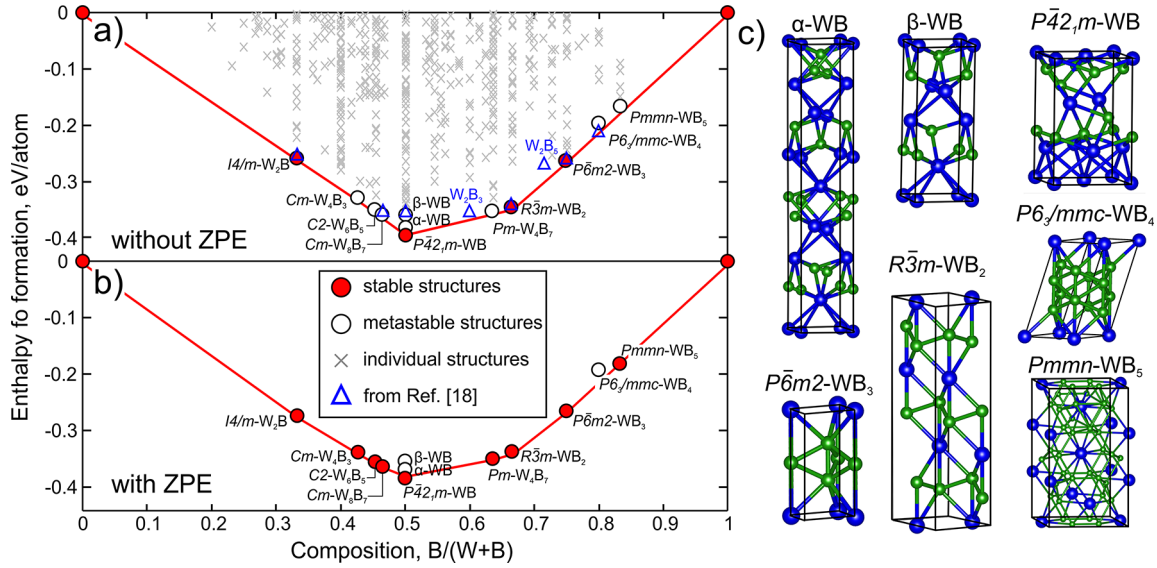

Figure 1. Thermodynamic convex hull of the W−B system (a) without and (b) with zero-point energy (ZPE) contribution. Filled circles are stable phases, open circles are metastable at 0 K, and open triangles are phases from ref 18. (c) Crystal structures of α-WB, β-WB, $P\bar{4}2_1m$-WB, and boron-rich $R\bar{3}m$-WB_2, $P\bar{6}m2$-WB_3, $P6_3/mmc$-WB_4, and $Pmmn$-WB_5 phases. Crystal structures of the predicted phases were visualized using VESTA.[60]

Table 1. Mechanical Properties of Predicted W−B Phases at 0 K[a]

phase	B	G	H_V	K_{IC}	phase	B	G	H_V	K_{IC}
$I4/m$-W_2B	337	153	12.1	3.45	WB_2 (exp)[14]	372		27.7	
W_2B[18]	338	155	12.4		WB_2 (exp)[20]			21.3	
Cm-W_4B_3	335	206	22.7	3.95	$P\bar{6}m2$-WB_3	308	226	30.1	3.79
$C2$-W_6B_5	337	203	21.7	3.91	WB_3[61]	294	240	35.9	
Cm-W_8B_7	338	195	19.9	3.82	WB_3[62]	295	252	43.1	
α-WB	349	192	18.5	3.82	$P6_3/mmc$-WB_4	325	212	24.8	3.73
α-WB[18]	352	199	19.8		WB_4[18]	299	217	29.0	
α-WB (exp)[20]			25.3		WB_4[62]	300	102	16.8	
β-WB	300	192	22.7	3.55	WB_4 (exp)[16]	339		28.1−43.3	
β-WB[18]	351	190	18		WB_4 (exp)[14]	304		31.8	
$P\bar{4}2_1m$-WB	314	245	34.3	4.12	$Pmmn$-WB_5	287	266	45.1	4.01
Pm-W_4B_7	325	250	34.3	4.16	$P\bar{6}m2$-WC	383	292	29.6	5.37
$R\bar{3}m$-WB_2	313	248	35.8	4.06	WC[63]	383	291		
WB_2[18]	318	266	39.7		WC (exp)[64]	439	302	30	
WB_2[61]	321	274	41.3						

[a]The bulk (B) and shear (G) moduli and Vickers hardness (H_V) are in GPa, and the fracture toughness (K_{IC}) is in MPa·m$^{0.5}$. Experimental values are at room temperature.

(5−8 MPa·m$^{0.5}$[55,56]) for WC, 3.3 MPa·m$^{0.5}$ (4−5 MPa·m$^{0.5}$[55]) for TiN, and 5.41 MPa·m$^{0.5}$ (2−5 MPa·m$^{0.5}$[50,54]) for c-BN.

With USPEX, we calculated the convex hull diagram of the W−B system (see Figure 1a), which displays all experimentally known phases, as well as several new phases (Cm-W_4B_3, $C2$-W_6B_5, Pm-W_4B_7, and $Pmmn$-WB_5). By definition, a thermodynamically stable phase has lower Gibbs free energy (or, at zero Kelvin, lower enthalpy) than any phase or phase assembly of the same composition. Phases that are located on the convex hull are thus by definition stable.

Let us first consider the case of T = 0 K. For WB, we found both known WB phases, namely, α and β, with a difference of enthalpy of about 15 meV/atom. Their crystal structures are in good agreement with experiment and so is the enthalpy difference, which is 13 meV/atom in experiment.[57] Moreover at zero Kelvin, the new $P\bar{4}2_1m$-WB was found to be thermodynamically more stable than α-WB, with an enthalpy difference of 12 meV/atom. Some of the phases predicted in ref 18 are found to be metastable (W_2B_3, W_2B_5, WB_4). We also predicted several phases with W:B ratios (4:3, 6:5, and 8:7) close to WB, while W_4B_7 is stoichiometrically close to WB_2. We find strong similarities between crystal structures of Cm-W_4B_3, $C2$-W_6B_5, Cm-W_8B_7, and β-WB (see Figure S2a in the Supporting Information). There is an open question about the existence of boron-rich tungsten borides WB_x with $x > 3$. Previously, WB_3 and WB_4 were predicted.[18,58] Here we predict that WB_4 found in ref 18 is metastable, being above the convex hull by 37 meV/atom if one neglects zero-point energy, and remains metastable when the zero-point energy is taken into account (see Figure 1a). Another new boron-rich phase, $Pmmn$-WB_5, seen both in our present calculations and in the calculations of the Guangzhou group,[59] was found to be metastable by 15 meV/atom (see Figure 1a) if one neglects the zero-point energy but becomes stable when the zero-point energy is taken into account (see Figure 1b).

DOI: 10.1021/acs.jpclett.8b01262
J. Phys. Chem. Lett. 2018, 9, 3470−3477

Crystal structures of α-WB, β-WB, $P\bar{4}2_1m$-WB, WB_2, WB_3, WB_4, and WB_5 are shown in Figure 1c. Structurally, α- and β-WB differ by the relative location of the layers. α-WB is made of AB-stacked WB layers, every other layer being rotated by 90°, while β-WB has AA′ stacking, where every other layer is shifted by half of the lattice parameter a (see Figure S1 in the Supporting Information). In both phases, each W is coordinated by 7 B atoms and 10 W atoms, with a total coordination number of 17. New $P\bar{4}2_1m$-WB has such layers as well, but each layer here is obtained by fusing of A and B layers of α-WB (see Figure S1 in the Supporting Information). Each layer consists of two tungsten atoms, one of which is coordinated by 8 B atoms and 8 W atoms, while the second one is coordinated by 6 B atoms and 10 W atoms. Crystal structures of all predicted phases are shown in Table S1 (see the Supporting Information). WB_3 has a hexagonal unit cell with one tungsten atom coordinated by eight boron atoms and six tungsten atoms. WB_5 has a very unusual structure, made of edge- and face-sharing WB_{12} hexagonal prisms (i.e., each W atom is coordinated by 12 B atoms) and open B_{15} clusters linked by B−B bonds into a 3D-structure (see Figure S3 in the Supporting Information for details).

Next we studied the mechanical properties of all predicted phases. We calculated the elastic constants tensor from which the hardness and fracture toughness were computed (see Table S2 in the Supporting Information). It is important to note that β-WB-based phases (Cm-W_4B_3, $C2$-W_6B_5, and Cm-W_8B_7) display similar to β-WB elastic properties and hardness. This comes from the structural similarity of these phases (see Figure S2 in the Supporting Information). Boron-rich phases WB_2 and WB_3 have high hardness of 40 and 30 GPa, respectively, both of which are in good agreement with experimental data (see Table 1). The highest Vickers hardness is for WB_5 and equals 45.1 GPa, i.e., this is a superhard material.

Comparison of the mechanical properties of the predicted phases with WC (the most used hard phase) indicates that most of the new W−B phases surpass WC by Vickers hardness, while many have comparable fracture toughness. The unique combination of Vickers hardness and fracture toughness makes tungsten borides promising materials for widespread use.

The most interesting material for different industrial applications is superhard WB_5, which has an extremely high Vickers hardness along with good fracture toughness (see Table 1). In this case, addition of the metal atom does not lead to reduction of the hardness (in comparison with pure boron) but significantly increases fracture toughness.

On the basis of the obtained data, we constructed an Ashby plot of the Vickers hardness vs fracture toughness, which allows one to clearly find materials with an optimal combination of these properties (see Figure 2). Predicted phases are denoted by red circles, while blue ones are known superhard materials (diamond, α-B, c-BN) and hard alloys (WC, TiN). All predicted phases were divided into two groups; see Figure 2. It can be clearly seen that all materials that are in the red region have a Vickers hardness higher than that for WC (horizontal line) together with high fracture toughness comparable to that of WC and TiN. Phases in the blue region have Vickers hardness < 30 GPa and lower fracture toughness and will be of limited practical use.

The ideal tensile and shear strengths have also been proposed as a measure of hardness.[65,66] We simulated the stress−strain curves for WB_3 and WB_5 (Figure 3). The lattice vectors of both phases were incrementally deformed in the direction of applied strain. At each step, the structure was relaxed such that all components of the Hellmann−Feynman stress tensor orthogonal to the applied stress were less than 0.01 GPa. The minimum tensile and shear stresses in the stress−strain curves are taken as the ideal tensile and shear strength.

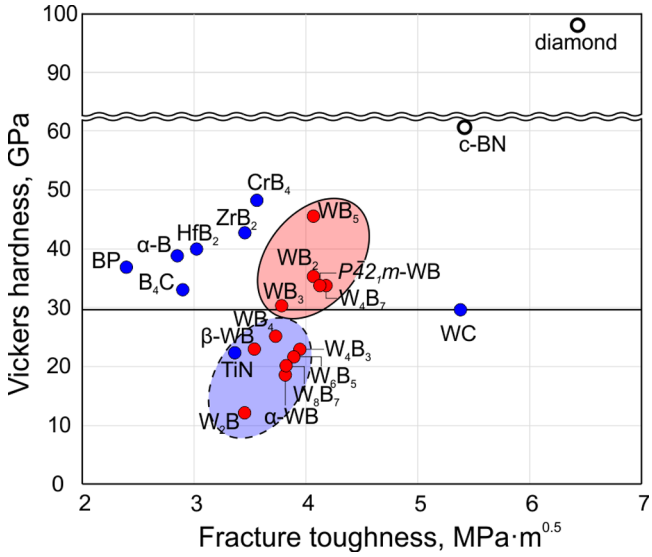

Figure 2. Ashby plot of Vickers hardness vs fracture toughness for predicted W−B phases (red points) compared with those of known superhard materials (blue points). The horizontal line is the value of the Vickers hardness of WC.

For tension of WB_3 (see Figure 3a), stress increases steeply with an ideal strength 52 GPa. Considering shear deformations of WB_3, the ideal shear strength corresponds to $(1\bar{1}0)[001]$ deformation with an ideal strength of 28 GPa (see Figure 3a). The ideal tensile strength of WB_5 was found along the [011] direction with a value of 54 GPa (see Figure 3b). Shear deformation shows lower values of ideal shear strength with an average value of 33 GPa (see Figure 3c). The minimum tensile and shear ideal strengths of WB_3 and WB_5 are thus 28 and 33 GPa, respectively.

As was mentioned above, WB_5 is thermodynamically stable at 0 K and zero pressure and is stabilized by the zero-point energy—a subtle effect; therefore, we performed a detailed study of the thermal stability of all predicted W−B phases along with WB_5 to see if this phase is stabilized by temperature or pressure.

First, we checked the effect of pressure and found that it destabilizes WB_5. A detailed study of the effect of pressure on the stability of tungsten borides will be reported elsewhere.[59] Then, we turned to investigating the effect of temperature by calculating the Gibbs free energy of each phase using both quasiharmonic (QHA) and anharmonic (AHA) approximations (see eqs 3 and 5). Gibbs free energies were calculated in the temperature range from 0 to 2500 K (melting temperatures of α-B and W are about 2400 and 3200 K,[67] respectively) with an increment of 100 K. It is generally accepted that the stable phase of boron at ambient pressure is the β-phase, but its structure is disordered and difficult to model; here we use α-B, which has practically indistinguishable energy.[68,69] As a result, we constructed phase diagrams in the composition−temperature space; see Figure 4. Hitherto unobserved $P\bar{4}2_1m$-WB turns out to be thermodynamically stable only at low temperatures from 0 to 300 K both within QHA and AHA

DOI: 10.1021/acs.jpclett.8b01262
J. Phys. Chem. Lett. 2018, 9, 3470−3477

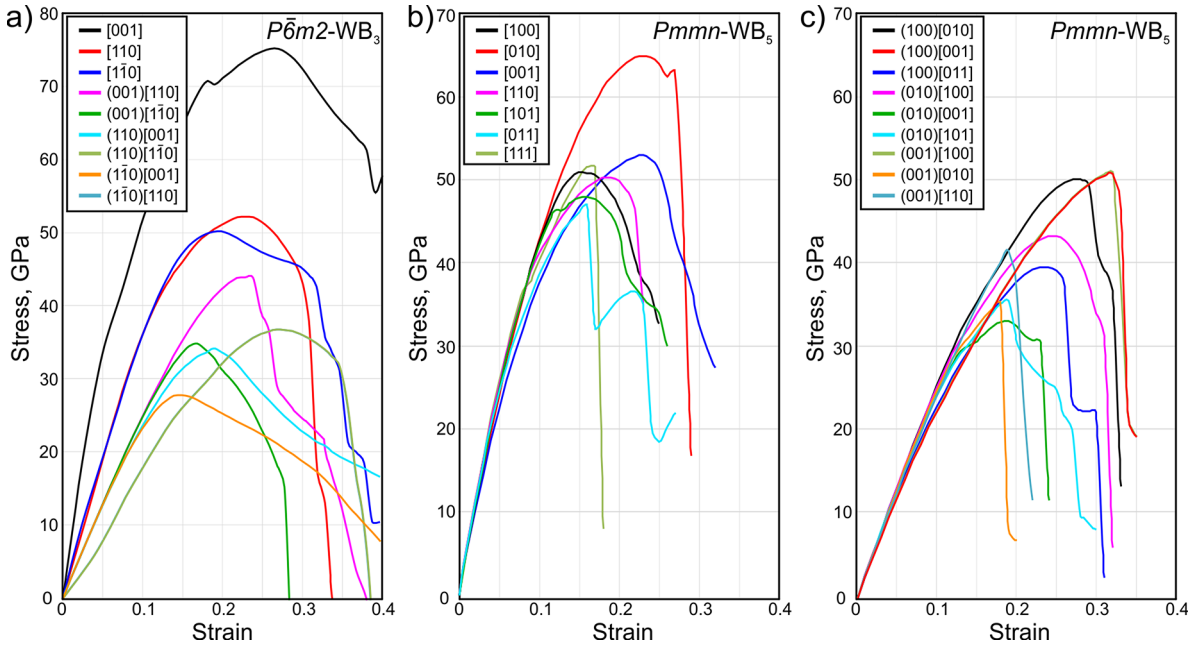

Figure 3. Ideal stress−strain curves of (a) $P\bar{6}m2$-WB_3 and (b,c) *Pmmn*-WB_5 along high-symmetry tensile and shear deformation directions.

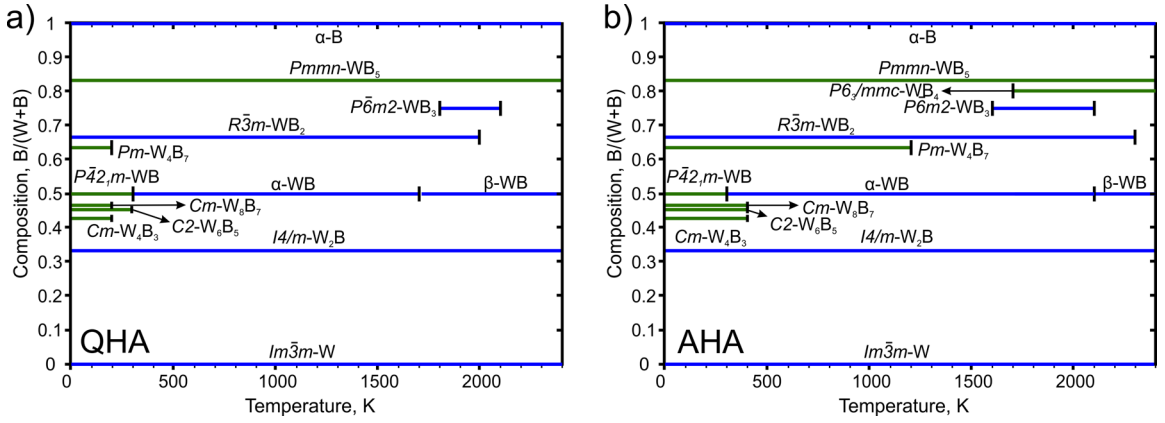

Figure 4. Temperature−composition phase diagrams calculated using (a) QHA and (b) AHA. New phases are shown by green color. These are simplified phase diagrams, not considering configurational entropy, finite homogeneity regions, and melting (congruent, incongruent, eutectic).

(see Figure 4). At temperatures above 300 K, α-WB is more stable. This low-temperature phase could not be observed in experiments because synthesis of WB is done at high temperatures (where α-B or β-B are stable), and at conditions where $P\bar{4}2_1m$-WB is stable (T < 300 K), kinetics are prohibitively slow for the transition to take place. One can see from Figure 4a that within the QHA, α-WB transforms to β-WB at $T \approx$ 1700 K, while within the AHA this transition occurs at 2100 K (see Figure 4b), which perfectly agrees with the experimental value of the transition temperature of 2110 K.[57]

Phases related to β-WB (*Cm*-W_4B_3, *C*2-W_6B_5, and *Cm*-W_8B_7) within the QHA are found to be stable only at temperatures below 300 K (see Figure 4a). AHA extends their temperature ranges of stability to 400 K (see Figure 4b). Similar stabilization due to anharmonicity is found for W_4B_7, which is a defective relative to $R\bar{3}m$-WB_2. Configurational entropy will further stabilize defective versions of WB (W_4B_3, W_6B_5, and W_8B_7) and WB_2 (W_4B_7) and merge WB_{1-x} and WB_{2-x} into just two phases, and it is possible that samples of WB and WB_2 actually contain a significant concentration of boron vacancies.

WB_3 shows a very narrow stability region within QHA, from 1800 to 2100 K (1600−2100 K in AHA). Neither QHA nor AHA show the appearance of WB_4 at any temperature. Newly predicted WB_5 is thermodynamically stable in the whole temperature range studied here, i.e., this phase is stable at least up to 2400 K (see Figure 4), implying that WB_5 can be synthesized. This also allows the use of WB_5 at very high temperatures, while WB_2 and WB_3 become unstable at such high temperatures (~2000 K).

In addition to thermodynamic stability, an important issue related to temperature is the temperature dependence of the mechanical properties of hard W−B phases. In Figure 5a,b, the temperature dependences of the elastic constants C_{ij} for WB_3 and WB_5 (within both QHA and AHA) are shown. Here one can see that all elastic constants depend on temperature nonlinearly. The same behavior was observed previously for Al_2O_3,[70] Mo, and W.[42] At 2000 K, WB_5 is predicted to have a hardness of 27 GPa, still a very high value.

In conclusion, we studied in detail the W−B system using global optimization algorithm USPEX and predicted new interesting materials. We found *Cm*-W_4B_3, *C*2-W_6B_5, *Pm*-W_4B_7,

DOI: 10.1021/acs.jpclett.8b01262
J. Phys. Chem. Lett. 2018, 9, 3470−3477

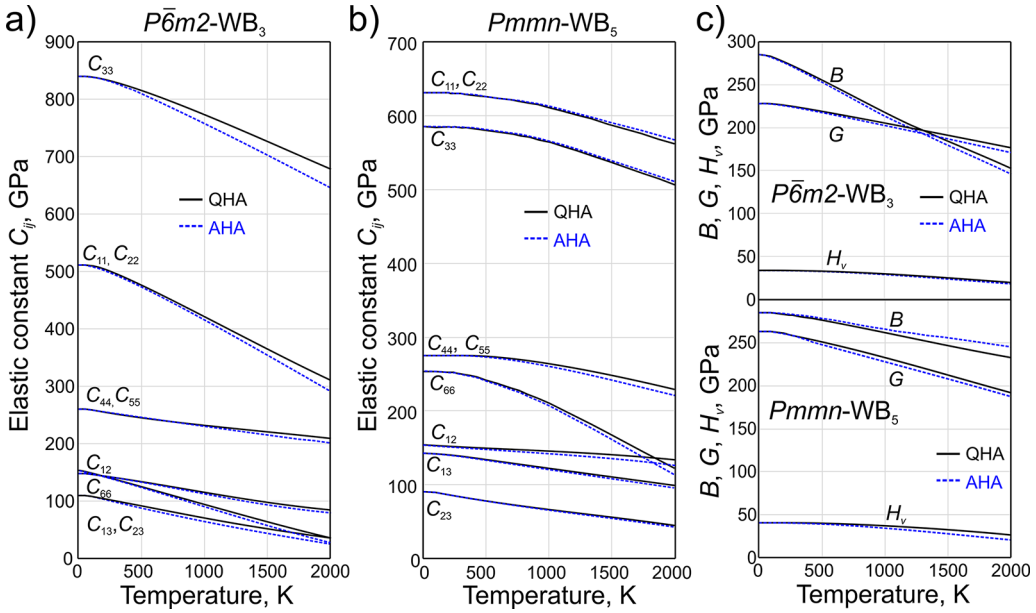

Figure 5. Temperature dependence of (a,b) C_{ij} and (c) bulk, shear moduli and the Vickers hardness of WB_3 and WB_5. Data calculated by QHA and AHA are shown by solid black and dotted blue lines, respectively.

and *Pmmn*-WB_5 phases. Among the predicted new phases, WB_5 is superhard and has a Vickers hardness of 45 GPa and a very high fracture toughness (4 MPa × $m^{0.5}$). In addition to its phenomenal mechanical properties, WB_5 is thermodynamically stable at ambient pressure at all temperatures up to at least 2400 K. Even though the mechanical properties of WB_5 are predicted to naturally decrease with temperature, WB_5 will possess impressive mechanical properties even at very high temperatures. All obtained data allow one to consider WB_5 as a promising material for applications in different fields of industry.

■ ASSOCIATED CONTENT

Supporting Information

The Supporting Information is available free of charge on the ACS Publications website at DOI: 10.1021/acs.jpclett.8b01262.

Crystal structure information of predicted phases, elastic constant tensors, and acoustic velocities (PDF)

■ AUTHOR INFORMATION

Corresponding Authors

*E-mail: A.Kvashnin@skoltech.ru (A.G.K.).
*E-mail: A.Oganov@skoltech.ru (A.R.O.).

ORCID

Alexander G. Kvashnin: 0000-0002-0718-6691

Notes

The authors declare no competing financial interest.

■ ACKNOWLEDGMENTS

The work was supported by the Russian Science Foundation (Grant No. 17-73-20038). This work received financial support from LLC "Gazpromneft-STC" under a commercial contract with Skoltech signed for the period Oct 1, 2017−Oct 1, 2018 entitled "Search for new superhard materials for drill bit cutters". Calculations were performed on the Rurik supercomputer of our laboratory at MIPT.

■ REFERENCES

(1) Solozhenko, V. L.; Dub, S. N.; Novikov, N. V. Mechanical Properties of Cubic BC2N, a New Superhard Phase. *Diamond Relat. Mater.* **2001**, *10* (12), 2228−2231.

(2) Solozhenko, V. L.; Gregoryanz, E. Synthesis of Superhard Materials. *Mater. Today* **2005**, *8* (11), 44−51.

(3) Solozhenko, V. L.; Kurakevych, O. O.; Andrault, D.; Le Godec, Y.; Mezouar, M. Ultimate Metastable Solubility of Boron in Diamond: Synthesis of Superhard Diamondlike BC5. *Phys. Rev. Lett.* **2009**, *102* (1), 015506.

(4) Blank, V. D.; Buga, S. G.; Serebryanaya, N. R.; Dubitsky, G. A.; Mavrin, B. N.; Popov, M. Y.; Bagramov, R. H.; Prokhorov, V. M.; Sulyanov, S. N.; Kulnitskiy, B. A.; et al. Structures and Physical Properties of Superhard and Ultrahard 3D Polymerized Fullerites Created from Solid C60 by High Pressure High Temperature Treatment. *Carbon* **1998**, *36* (5−6), 665−670.

(5) Li, Q.; Ma, Y.; Oganov, A. R.; Wang, H.; Wang, H.; Xu, Y.; Cui, T.; Mao, H.-K.; Zou, G. Superhard Monoclinic Polymorph of Carbon. *Phys. Rev. Lett.* **2009**, *102* (17), 175506−175510.

(6) He, C.; Sun, L.; Zhang, C.; Peng, X.; Zhang, K.; Zhong, J. New Superhard Carbon Phases between Graphite and Diamond. *Solid State Commun.* **2012**, *152* (16), 1560−1563.

(7) Han, L.; Wang, S.; Zhu, J.; Han, S.; Li, W.; Chen, B.; Wang, X.; Yu, X.; Liu, B.; Zhang, R.; et al. Hardness, Elastic, and Electronic Properties of Chromium Monoboride. *Appl. Phys. Lett.* **2015**, *106*, 221902.

(8) Zhong, M.-M.; Huang, C.; Tian, C.-L. The Structural Stabilities, Mechanical Properties and Hardness of Chromium Tetraboride: Compared with Low-B Borides. *Int. J. Mod. Phys. B* **2016**, *30*, 1650201.

(9) Kvashnin, A. G.; Oganov, A. R.; Samtsevich, A. I.; Allahyari, Z. Computational Search for Novel Hard Chromium-Based Materials. *J. Phys. Chem. Lett.* **2017**, *8* (4), 755−764.

(10) Zhong, M.-M.; Kuang, X.-Y.; Wang, Z.-H.; Shao, P.; Ding, L.-P.; Huang, X.-F. Phase Stability, Physical Properties, and Hardness of Transition-Metal Diborides MB2 (M = Tc, W, Re, and Os): First-Principles Investigations. *J. Phys. Chem. C* **2013**, *117*, 10643−10652.

(11) Zhang, M.; Wang, H.; Wang, H.; Cui, T.; Ma, Y. Structural Modifications and Mechanical Properties of Molybdenum Borides from First Principles. *J. Phys. Chem. C* **2010**, *114* (14), 6722−6725.

(12) Liang, Y.; Yuan, X.; Fu, Z.; Li, Y.; Zhong, Z. An Unusual Variation of Stability and Hardness in Molybdenum Borides. *Appl. Phys. Lett.* **2012**, *101* (18), 181908.

DOI: 10.1021/acs.jpclett.8b01262
J. Phys. Chem. Lett. 2018, 9, 3470−3477

(13) Itoh, H.; Matsudaira, T.; Naka, S.; Hamamoto, H.; Obayashi, M. Formation Process of Tungsten Borides by Solid State Reaction between Tungsten and Amorphous Boron. *J. Mater. Sci.* **1987**, *22* (8), 2811−2815.
(14) Gu, Q.; Krauss, G.; Steurer, W. Transition Metal Borides: Superhard versus Ultra-Incompressible. *Adv. Mater.* **2008**, *20* (19), 3620−3626.
(15) Zhao, E.; Meng, J.; Ma, Y.; Wu, Z. Phase Stability and Mechanical Properties of Tungsten Borides from First Principles Calculations. *Phys. Chem. Chem. Phys.* **2010**, *12* (40), 13158−13165.
(16) Mohammadi, R.; Lech, A. T.; Xie, M.; Weaver, B. E.; Yeung, M. T.; Tolbert, S. H.; Kaner, R. B. Tungsten Tetraboride, an Inexpensive Superhard Material. *Proc. Natl. Acad. Sci. U. S. A.* **2011**, *108* (27), 10958−10962.
(17) Aydin, S.; Ciftci, Y. O.; Tatar, A. Superhard Transition Metal Tetranitrides: XN4 (X = Re, Os, W). *J. Mater. Res.* **2012**, *27* (13), 1705−1715.
(18) Cheng, X.-Y.; Chen, X.-Q.; Li, D.-Z.; Li, Y.-Y. Computational Materials Discovery: The Case of the W−B System. *Acta Crystallogr., Sect. C: Struct. Chem.* **2014**, *70* (2), 85−103.
(19) Kiessling, R.; et al. The Crystal Structures of Molybdenum and Tungsten Borides. *Acta Chem. Scand.* **1947**, *1*, 893−916.
(20) Okada, S. Preparations and Some Properties of W2B, δ-WB and WB2 Crystals from High-Temperature Metal Solutions. *Jpn. J. Appl. Phys.* **1995**, *34* (1R), 226.
(21) Woods, H. P.; Wawner, F. E.; Fox, B. G. Tungsten Diboride: Preparation and Structure. *Science* **1966**, *151* (3706), 75−75.
(22) Chen, X.-Q.; Fu, C. L.; Krčmar, M.; Painter, G. S. Electronic and Structural Origin of Ultraincompressibility of 5d Transition-Metal Diborides MB2 (M = W, Re, Os). *Phys. Rev. Lett.* **2008**, *100* (19), 196403.
(23) Zhang, H.-Y.; Xi, F.; Zeng, Z.-Y.; Chen, X.-R.; Cai, L.-C. First-Principles Predictions of Phase Transition and Mechanical Properties of Tungsten Diboride under Pressure. *J. Phys. Chem. C* **2017**, *121* (13), 7397−7403.
(24) Frotscher, M.; Klein, W.; Bauer, J.; Fang, C.-M.; Halet, J.-F.; Senyshyn, A.; Baehtz, C.; Albert, B. M2B5 or M2B4? A Reinvestigation of the Mo/B and W/B System. *Z. Anorg. Allg. Chem.* **2007**, *633* (15), 2626−2630.
(25) Veblen, D. R. Polysomatism and Polysomatic Series: A Review and Applications. *Am. Minaralogist* **1991**, *76*, 801−826.
(26) Kayhan, M.; Hildebrandt, E.; Frotscher, M.; Senyshyn, A.; Hofmann, K.; Alff, L.; Albert, B. Neutron Diffraction and Observation of Superconductivity for Tungsten Borides, WB and W2B4. *Solid State Sci.* **2012**, *14* (11), 1656−1659.
(27) Oganov, A. R.; Glass, C. W. Crystal Structure Prediction Using Ab Initio Evolutionary Techniques: Principles and Applications. *J. Chem. Phys.* **2006**, *124*, 244704.
(28) Oganov, A. R.; Ma, Y.; Lyakhov, A. O.; Valle, M.; Gatti, C. Evolutionary Crystal Structure Prediction as a Method for the Discovery of Minerals and Materials. *Rev. Mineral. Geochem.* **2010**, *71*, 271−298.
(29) Oganov, A. R.; Lyakhov, A. O.; Valle, M. How Evolutionary Crystal Structure Prediction Works—and Why. *Acc. Chem. Res.* **2011**, *44*, 227−237.
(30) Hohenberg, P.; Kohn, W. Inhomogeneous Electron Gas. *Phys. Rev.* **1964**, *136* (3B), B864−B871.
(31) Kohn, W.; Sham, L. J. Self-Consistent Equations Including Exchange and Correlation Effects. *Phys. Rev.* **1965**, *140* (4), A1133−A1138.
(32) Perdew, J. P.; Burke, K.; Ernzerhof, M. Generalized Gradient Approximation Made Simple. *Phys. Rev. Lett.* **1996**, *77* (18), 3865−3868.
(33) Blöchl, P. E. Projector Augmented-Wave Method. *Phys. Rev. B: Condens. Matter Mater. Phys.* **1994**, *50* (24), 17953−17979.
(34) Kresse, G.; Joubert, D. From Ultrasoft Pseudopotentials to the Projector Augmented-Wave Method. *Phys. Rev. B: Condens. Matter Mater. Phys.* **1999**, *59* (3), 1758−1775.
(35) Kresse, G.; Hafner, J. Ab Initio Molecular Dynamics for Liquid Metals. *Phys. Rev. B: Condens. Matter Mater. Phys.* **1993**, *47* (1), 558−561.
(36) Kresse, G.; Hafner, J. Ab Initio Molecular-Dynamics Simulation of the Liquid-Metal-Amorphous-Semiconductor Transition in Germanium. *Phys. Rev. B: Condens. Matter Mater. Phys.* **1994**, *49* (20), 14251−14269.
(37) Kresse, G.; Furthmüller, J. Efficient Iterative Schemes for Ab Initio Total-Energy Calculations Using a Plane-Wave Basis Set. *Phys. Rev. B: Condens. Matter Mater. Phys.* **1996**, *54* (16), 11169−11186.
(38) Monkhorst, H. J.; Pack, J. D. Special Points for Brillouin-Zone Integrations. *Phys. Rev. B* **1976**, *13* (12), 5188−5192.
(39) Kern, G.; Kresse, G.; Hafner, J. Ab Initio Calculation of the Lattice Dynamics and Phase Diagram of Boron Nitride. *Phys. Rev. B: Condens. Matter Mater. Phys.* **1999**, *59*, 8551−8559.
(40) Togo, A.; Tanaka, I. First Principles Phonon Calculations in Materials Science. *Scr. Mater.* **2015**, *108*, 1−5.
(41) Togo, A.; Oba, F.; Tanaka, I. First-Principles Calculations of the Ferroelastic Transition between Rutile-Type and CaCl2-Type SiO2 at High Pressures. *Phys. Rev. B: Condens. Matter Mater. Phys.* **2008**, *78*, 134106.
(42) Guillermet, A. F.; Grimvall, G. Analysis of Thermodynamic Properties of Molybdenum and Tungsten at High Temperatures. *Phys. Rev. B: Condens. Matter Mater. Phys.* **1991**, *44* (9), 4332−4340.
(43) Wallace, D. C. *Thermodynamics of Crystals*; Courier Corporation, 1998.
(44) Sanjurjo, J. A.; López-Cruz, E.; Vogl, P.; Cardona, M. Dependence on Volume of the Phonon Frequencies and the Ir Effective Charges of Several III-V Semiconductors. *Phys. Rev. B: Condens. Matter Mater. Phys.* **1983**, *28* (8), 4579−4584.
(45) Chen, X.-Q.; Niu, H.; Li, D.; Li, Y. Modeling Hardness of Polycrystalline Materials and Bulk Metallic Glasses. *Intermetallics* **2011**, *19*, 1275−1281.
(46) Hill, R. The Elastic Behaviour of a Crystalline Aggregate. *Proc. Phys. Soc., London, Sect. A* **1952**, *65* (5), 349.
(47) Anderson, O. L. A Simplified Method for Calculating the Debye Temperature from Elastic Constants. *J. Phys. Chem. Solids* **1963**, *24* (7), 909−917.
(48) Popov, M.; Kulnitskiy, B.; Blank, V. 3.20 - Superhard Materials Based on Fullerenes and Nanotubes A2 - Sarin. In *Comprehensive Hard Materials*; Vinod, K., Ed.; Elsevier: Oxford, 2014; pp 515−538.
(49) Stone, D. S.; Yoder, K. B.; Sproul, W. D. Hardness and Elastic Modulus of TiN Based on Continuous Indentation Technique and New Correlation. *J. Vac. Sci. Technol., A* **1991**, *9* (4), 2543−2547.
(50) Solozhenko, V. L.; Kurakevych, O. O.; Le Godec, Y. Creation of Nanostuctures by Extreme Conditions: High-Pressure Synthesis of Ultrahard Nanocrystalline Cubic Boron Nitride. *Adv. Mater.* **2012**, *24* (12), 1540−1544.
(51) Niu, H.; Oganov, A. R. Fracture Toughness Prediction of Crystal by First-Principles Calculations. *Phys. Rev. Lett.* **2018**, Submitted.
(52) Drory, M. D.; Dauskardt, R. H.; Kant, A.; Ritchie, R. O. Fracture of Synthetic Diamond. *J. Appl. Phys.* **1995**, *78* (5), 3083−3088.
(53) Dubrovinskaia, N.; Dub, S.; Dubrovinsky, L. Superior Wear Resistance of Aggregated Diamond Nanorods. *Nano Lett.* **2006**, *6* (4), 824−826.
(54) Brookes, C. A. Mechanical Properties of Cubic Boron Nitride − a Perspective View. *Institute of Physics, Conference Series* **1986**, *75*, 207−220.
(55) Munro, R. G.; Freiman, S. W.; Baker, T. L. *Fracture Toughness Data for Brittle Materials*; U.S. Dept. of Commerce, National Institute of Standards and Technology: Gaithersburg, MD, 1998.
(56) Groover, M. P. *Fundamentals of Modern Manufacturing: Materials, Processes, and Systems*; John Wiley & Sons, 2010.
(57) Duschanek, H.; Rogl, P. Critical Assessment and Thermodynamic Calculation of the Binary System Boron-Tungsten (B-W). *J. Phase Equilib.* **1995**, *16* (2), 150−161.

DOI: 10.1021/acs.jpclett.8b01262
J. Phys. Chem. Lett. 2018, 9, 3470−3477

(58) Cheng, X.; Zhang, W.; Chen, X.-Q.; Niu, H.; Liu, P.; Du, K.; Liu, G.; Li, D.; Cheng, H.-M.; Ye, H.; et al. Interstitial-Boron Solution Strengthened WB3+x. *Appl. Phys. Lett.* **2013**, *103* (17), 171903.
(59) Zhao, Z.; Duan, Y.; Gao, J.; Liu, W.; Dong, H.; Dong, H.; Zhang, D.; Oganov, A. R. Unexpected Stable Phases of Tungsten Borides. **2018**, Submitted.
(60) Momma, K.; Izumi, F. VESTA 3 for Three-Dimensional Visualization of Crystal, Volumetric and Morphology Data. *J. Appl. Crystallogr.* **2011**, *44*, 1272−1276.
(61) Liang, Y.; Zhong, Z.; Zhang, W. A Thermodynamic Criterion for Designing Superhard Transition-Metal Borides with Ultimate Boron Content. *Comput. Mater. Sci.* **2013**, *68* (Supplement C), 222−228.
(62) Liang, Y.; Fu, Z.; Yuan, X.; Wang, S.; Zhong, Z.; Zhang, W. An Unexpected Softening from WB 3 to WB 4. *EPL Europhys. Lett.* **2012**, *98* (6), 66004.
(63) Liu, Y.; Jiang, Y.; Zhou, R.; Feng, J. Mechanical Properties and Chemical Bonding Characteristics of WC and W2C Compounds. *Ceram. Int.* **2014**, *40* (2), 2891−2899.
(64) *Landolt-Börnstein: Numerical Data and Functional Relationships in Science and Technology - New Series*, 2017.
(65) Roundy, D.; Krenn, C. R.; Cohen, M. L.; Morris, J. W. Ideal Shear Strengths of Fcc Aluminum and Copper. *Phys. Rev. Lett.* **1999**, *82* (13), 2713−2716.
(66) Roundy, D.; Krenn, C. R.; Cohen, M. L.; Morris, J. W., Jr. The Ideal Strength of Tungsten. *Philos. Mag. A* **2001**, *81* (7), 1725−1747.
(67) *Handbook of Chemistry and Physics*, 81st ed.; Lide, D. R., Ed.; CRC Press: Boca Raton, FL, 2000.
(68) van Setten, M. J.; Uijttewaal, M. A.; de Wijs, G. A.; de Groot, R. A. Thermodynamic Stability of Boron: The Role of Defects and Zero Point Motion. *J. Am. Chem. Soc.* **2007**, *129* (9), 2458−2465.
(69) Ogitsu, T.; Schwegler, E.; Galli, G. β-Rhombohedral Boron: At the Crossroads of the Chemistry of Boron and the Physics of Frustration. *Chem. Rev.* **2013**, *113* (5), 3425−3449.
(70) Shang, S.-L.; Zhang, H.; Wang, Y.; Liu, Z.-K. Temperature-Dependent Elastic Stiffness Constants of α- and θ-Al 2 O 3 from First-Principles Calculations. *J. Phys.: Condens. Matter* **2010**, *22* (37), 375403.

DOI: 10.1021/acs.jpclett.8b01262
J. Phys. Chem. Lett. 2018, 9, 3470−3477